Volume 6 | Number 6 | June 2018 | Pages 1273–1656

Biomaterials Science

rsc.li/biomaterials-science

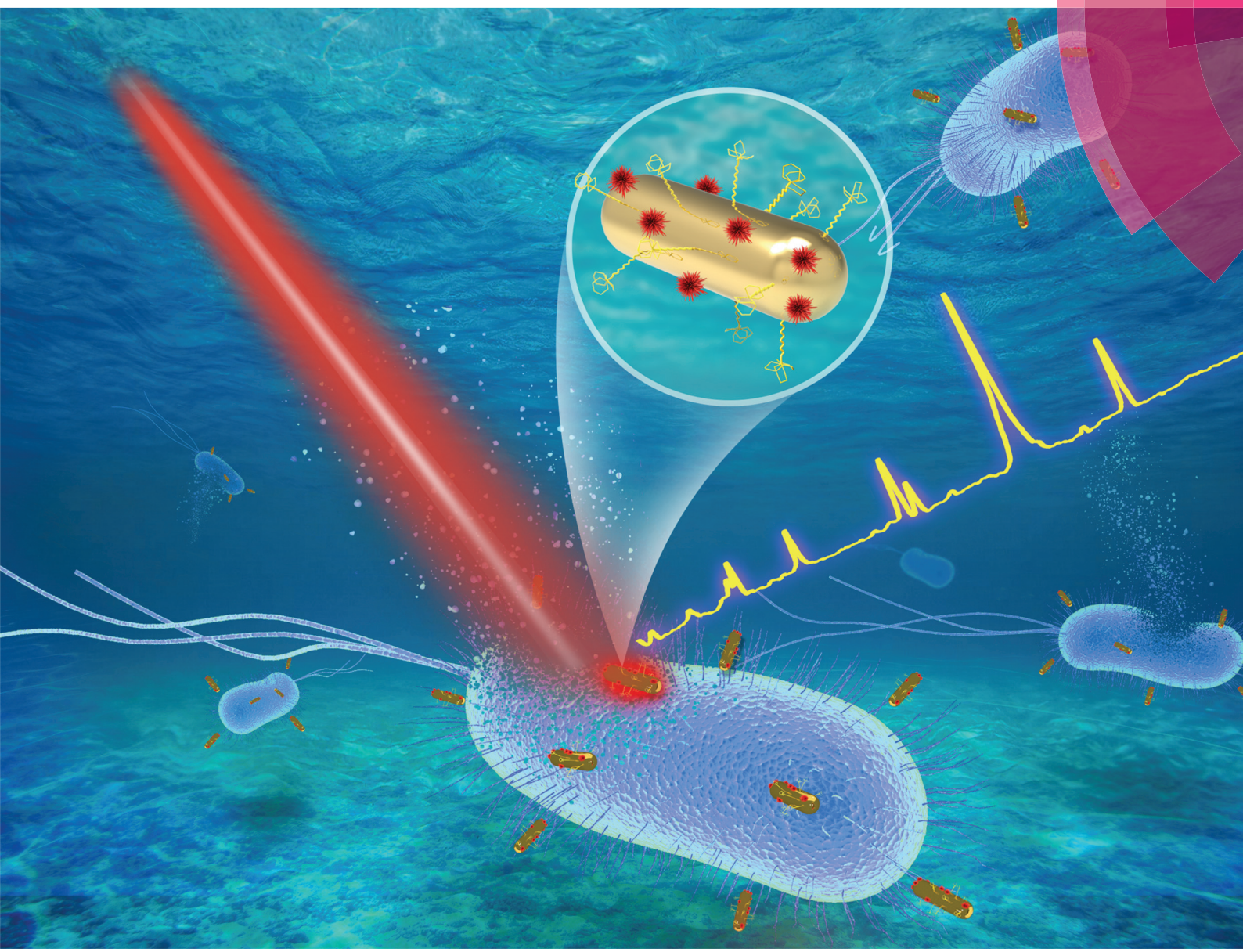

ISSN 2047-4849

ROYAL SOCIETY OF CHEMISTRY

PAPER
Hongwei Duan, Mary B. Chan-Park *et al.*
Raman-encoded, multivalent glycan-nanoconjugates for traceable specific binding and killing of bacteria

ESB European Society for Biomaterials

Biomaterials Science

PAPER

View Article Online
View Journal | View Issue

Check for updates

Cite this: *Biomater. Sci.*, 2018, **6**, 1339

Raman-encoded, multivalent glycan-nanoconjugates for traceable specific binding and killing of bacteria†

Surendra H. Mahadevegowda,‡[a] Shuai Hou,‡[a] Jielin Ma,[a] Damien Keogh,[a] Jianhua Zhang,[a] Asadulla Mallick,[b] Xue-Wei Liu,[b] Hongwei Duan *[a] and Mary B. Chan-Park *[a]

Received 4th February 2018,
Accepted 24th March 2018

DOI: 10.1039/c8bm00139a

rsc.li/biomaterials-science

Glycan recognition plays key roles in cell–cell and host–pathogen interactions, stimulating widespread interest in developing multivalent glycoconjugates with superior binding affinity for biological and medical uses. Here, we explore the use of Raman-encoded silver coated gold nanorods (GNRs) as scaffolds to form multivalent glycoconjugates. The plasmonic scaffolds afford high-loading of glycan density and their optical properties offer the possibilities of monitoring and quantitative analysis of glycan recognition. Using *E. coli* strains with tailored on/off of the FimH receptors, we have demonstrated that Raman-encoded GNRs not only allow for real-time imaging and spectroscopic detection of specific binding of the glycan–GNR conjugates with bacteria of interest, but also cause rapid eradication of the bacteria due to the efficient photothermal conversion of GNRs in the near-infrared spectral window. We envision that optically active plasmonic glycoconjugates hold great potential for screening multivalent glycan ligands for therapeutic and diagnostic applications.

Open Access Article. Published on 26 March 2018. Downloaded on 5/7/2026 1:40:22 AM.
This article is licensed under a Creative Commons Attribution-NonCommercial 3.0 Unported Licence.

Introduction

Glycan recognition is commonly involved in a diverse range of biological and pathological processes such as proliferation, differentiation, immune response, and microbial infections *via* cell–cell and host–pathogen interactions.[1] The interaction between individual carbohydrate ligands and protein receptors typically shows high specificity but low affinity, with dissociation constants in the millimolar range.[2] Nature has circumvented this problem by forming multivalent carbohydrate constructs to increase their binding affinity with proteins.[3] Multivalent glycoconjugates have been synthesized by the combination of carbohydrate head groups with different linkers and molecular or nanoscale scaffolds.[4–7] Nanoparticles, in particular metal nanoparticles,[8,9] magnetic nanoparticles,[10–12] and quantum dots,[13] have been employed to build multivalent glycoconjugates as they exhibit additional functionalities, which provide opportunities for magnetic separation of bacteria,[10] targeting tumoral cells,[14] inhibiting bacterial[15] or virus infections,[16,17] and detecting viruses.[18] Real-time monitoring and quantitative detection of the interactions of multivalent glycan constructs with protein receptors in living systems is crucial for the design of high-affinity multivalent glycan-nanoconjugates for therapeutic and diagnostic applications. However, common analytical methods such as haemagglutination inhibition assay,[19] isothermal microcalorimetry (ITC)[20] and surface plasmon resonance (SPR)[21] are limited to studies in solutions or at liquid–solid interfaces.

Here, we use silver-coated gold nanorods (GNRs) as scaffolds to anchor glycans and establish a model system for the quantitative study of the multivalent binding between glycan-functionalized GNRs and bacteria. Due to the unique shape effect, the GNRs exhibit a strong longitudinal localized surface plasmon resonance (LSPR), which is damped *via* radiative and nonradiative channels.[22] The radiative damping (light scattering) is easily detected using dark-field microscopy, which has been used for many bioimaging applications.[23] Additionally, LSPR is accompanied by the generation of an intense electromagnetic field near the metal surface, facilitating surface enhanced Raman scattering (SERS).[24–27] Finally, the nonradiative damping of the GNRs enables them to absorb light effectively and release heat into the environment. The

[a]*School of Chemical and Biomedical Engineering, Nanyang Technological University, 62 Nanyang Drive, Singapore 637459, Singapore. E-mail: hduan@ntu.edu.sg, mbechan@ntu.edu.sg*
[b]*Division of Chemistry and Biological Chemistry, School of Physical and Mathematical Sciences, Nanyang Technological University, 21 Nanyang Link, Singapore 637371, Singapore*

†Electronic supplementary information (ESI) available. See DOI: 10.1039/c8bm00139a

‡These authors contributed equally to this work.

Open Access Article. Published on 26 March 2018. Downloaded on 5/7/2026 1:40:22 AM.
This article is licensed under a Creative Commons Attribution-NonCommercial 3.0 Unported Licence.

absorption cross-section of the GNRs is four to six orders of magnitude larger than that of traditional dyes,[28] making them an efficient photothermal transducer. Taken together, GNRs enable microscopic and spectroscopic detection and quantification of the binding event, and they can also be used for photothermal killing of bacteria.[29]

In this study, uropathogenic *Escherichia coli* (UPEC), which expresses the mannose-specific FimH protein on its type 1 fimbriae,[30] has been chosen as a model bacterial system. UPEC causes urinary tract infection (UTI), which is one of the most prominent infectious diseases worldwide and affects 150 million people annually.[31–34] The FimH subunits bind to the mannose moiety of the host cell; therefore, mannose derivatives are frequently used for targeting UPEC. We studied the specificity and affinity of such glyco-GNRs using two well-controlled UPEC strains: FimH-ON bacteria that express the FimH protein, and FimH-OFF bacteria which are FimH-deficient. We first confirmed the multivalency effect of the glycan-modified GNRs in concanavalin A (ConA) recognition. We further explored the multivalent glycan–GNR nanoconjugates for bacteria recognition. Dark-field microscopy and Raman spectroscopy clearly reveal that the GNRs specifically bind to FimH-ON bacteria. Raman spectroscopy also allows us to measure the binding affinity. Furthermore, the photothermal release of heat from the GNRs to the targeted bacteria upon near-infrared (NIR) irradiation leads to nearly 100% killing of the bacteria. Our well-defined model system provides new strategies for quantitative analysis of glycan–protein interactions in bacterial systems. Moreover, the combination of glycans and plasmonic nanoparticles is a promising platform for efficient targeted detection and killing of bacteria.

Experimental section

General methods for glycocluster synthesis and characterization

All the reactions were performed using oven-dried glassware apparatus. All thiol–ene click reactions were performed using UV light of wavelength 365 nm under an argon atmosphere. Silica gel of mesh size 35–70 μm purchased from Merck Pte Ltd was used to perform column chromatography. ^{1}H, ^{13}C and DEPT-135 spectra were recorded using a Bruker AV 300 MHz NMR instrument. In ^{1}H NMR spectra, solvent residual peaks were set to 4.79 for D_2O, 7.26 for $CDCl_3$, and 3.31 for CD_3OD and in proton decoupled ^{13}C NMR spectra the middle peak of the solvent residual peak of $CDCl_3$ was set to 77.16, and for CD_3OD the middle peak was set to 49.00 ppm.

Synthesis of Au nanorods

Au seeds were prepared by the reduction of $HAuCl_4$ (0.25 mM, 5 mL) with $NaBH_4$ (10 mM, 0.3 mL) in an aqueous cetyltrimethylammonium bromide (CTAB) solution (100 mM) and aged for 2 h before use. An aliquot of the seed solution (0.6 mL) was added to a growth solution (250 mL) containing CTAB (100 mM), $HAuCl_4$ (0.5 mM), ascorbic acid (0.8 mM), aqueous $AgNO_3$ (0.12 mM), and aqueous HCl (19 mM). The mixture was left undisturbed at 30 °C for 4 h. The solution was centrifuged twice (8000 rcf, 10 min) and redispersed in water to obtain a final concentration of gold equal to 0.5 mM.

Synthesis of Raman dye modified Au@Ag nanorods (GNRs)

The Au nanorods were dispersed in a cetyltrimethylammonium chloride (CTAC) solution (10 mL, 10 mM). A DMF solution of the Raman dye, 4-nitrothiophenol, was added with a final concentration of 50 μM and the solution was incubated at 60 °C for 30 min. A solution of aqueous $AgNO_3$ (0.5 mL, 10 mM) and ascorbic acid (0.5 mL, 100 mM) was added into the Au nanorod solution. The mixture was allowed to react at 60 °C for 1 h. The average Ag shell thickness was 2.2 nm. The GNRs were collected by centrifugation at 6000 rcf for 10 min and redispersed in a 0.05% sodium dodecyl sulphate (SDS) solution.

Glycan-functionalization of GNRs

For a typical glycan-functionalization procedure, a solution of **Man_3-SH** (1 mM, 50 μL) was added into 950 μL of GNR solution with vigorous stirring. The mixture was kept for 3 h before centrifugation. The glycan-functionalized GNRs were further washed twice and dispersed in water.

Gel electrophoresis

The modification of the GNRs was evaluated by gel electrophoresis (Thermo Scientific EC 300XL) in 0.25% agarose gels using 1× 3-(*N*-morpholino)propanesulfonic acid (MOPS, pH 7.4) as the running buffer at 100 V for 10 min.

Photothermal efficiency evaluation of the nanorods

The GNR dispersions of different absorbance values (0.5 and 1) were irradiated using a NIR laser (808 nm, 1 W cm^{-2}). Water was used as a negative control. The temperature was monitored during heating. After the temperature reached equilibrium, the laser was switched off and the cooling process was monitored. Real-time thermal imaging of the samples was performed using a FLIR thermal camera. The photothermal conversion efficiency of the GNRs was calculated according to a method reported previously.[35]

ConA recognition

ConA was prepared in a 10 mM phosphate buffer (pH 7.4) containing 2 mM Mn^{2+} and 2 mM Ca^{2+}. ConA solutions of different concentrations were added into 1 mL of the Man_3-GNR or Gal_3-GNR solution. After incubation for 30 min, UV-vis extinction spectra of the solution were recorded. For a competitive assay, a mannose solution was first added into the Man_3-GNR solution, and then the ConA solution was added to reach a final concentration of 20 nM. The extinction spectra were measured after incubation for 30 min.

Isothermal calorimetric titration

Isothermal calorimetric titrations were carried out in a MICROCAL PEAQ-ITC instrument with a stirring speed of 750

 This journal is © The Royal Society of Chemistry 2018

Open Access Article. Published on 26 March 2018. Downloaded on 5/7/2026 1:40:22 AM.
This article is licensed under a Creative Commons Attribution-NonCommercial 3.0 Unported Licence.

rpm. Isothermal calorimetric titration was performed with 0.2 mM ConA concentration (molecular weight of 25 600 g mol^{-1}); methyl α-D-mannopyranoside (α-mmp) and Man_3-SH were used at 2 mM concentrations in 10 mM acetate buffer of pH = 4.8 containing metal salts of 10 mM NaCl, 1 mM $CaCl_2$ and 1 mM $MnSO_4$. The multivalency effect of Man_3-GNR in protein recognition was evaluated by titrating ligand mixtures of α-mmp and Man_3-GNR with ConA.

Bacterial strains and culture conditions

Escherichia coli UTI89 is an *E. coli* strain isolated from the urine of a cystitis patient (PMID 16585510). Phase locked ON (SLC-490) and OFF (SLC-492) mutants of UTI89 were provided by the lab of Swaine Chen (unpublished). Strains SLC-490 and SLC-492 were prepared by reversing the sequence of the left inverted repeat of the fimS invertible element in the chromosome using recombineering with a dual positive–negative selection cassette (PMID 25800749 and 10829079). *Escherichia coli* (*E. coli*, UTI89) was cultured in Luria–Bertani (LB) medium for 24 h at 37 °C without shaking. After 24 h, 10 μL of the solution was subcultured statically in 1 mL of LB medium for another 4 h. The static growth is essential for the expression of FimH. The bacteria were collected by centrifugation at 1500 rcf for 10 min and washed with PBS.

Dark-field imaging

A solution of Man_3-GNR (0.5 nM, 50 μL) was mixed with either FimH ON or FimH OFF *E. coli* (10^8 CFU mL^{-1}, 50 μL). After incubation for 1 h at 37 °C, the mixture was filtered using a centrifuge tube filter (pore size: 0.45 μm, 100 rcf, 10 min) to remove unbound GNRs. The bacteria were further washed twice using the same procedure and finally dispersed in 100 μL of water. 2 μL of the solution was dropped on a glass slide and covered by a coverslip. The sample was imaged using a dark-field microscope (Olympus IX71) with a 100× oil-immersed objective.

Raman spectroscopy

E. coli dispersions (0.5 mL, 10^8 CFU mL^{-1}) were mixed with 0.5 mL of Man_3-GNR solutions with increasing concentrations (final concentrations ranging from 0 to 0.5 nM). After incubation of 1 h, unbound GNRs were removed using the same procedures as described above. The collected filtrates were redispersed in water and the Raman spectra were obtained under the excitation of a 785 nm laser (10 mW).

Selective killing of *E. coli* UTI89 by photothermal effects of Au nanocomposites

E. coli dispersions (0.5 mL, 10^8 CFU mL^{-1}) were mixed with 0.5 mL of Man_3-GNR solutions with increasing concentrations (final concentrations ranging from 0 to 0.2 nM). After gently shaking for 1 h, unbound nanorods were removed using filtration as described above. The bacteria were then redispersed in 1 mL of PBS and exposed to a NIR laser (808 nm, 1 W cm^{-2}) for 15 min. The bacteria were transferred to LB agar plates, and incubated at 37 °C for 24 h and the colony number for each plate was counted.

Live/dead staining

Bacteria (10^8 CFU mL^{-1}) were prepared in a similar way as stated above. The samples were then stained with the LIVE/DEAD BacLight Bacterial Viability kit for 15 min at room temperature and the bacterial viability was assessed by using an Olympus IX71 inverted microscope with a 20× objective.

Transmission electron microscopy (TEM)

Man_3-GNR (0.2 nM) was mixed with *E. coli* and incubated for 1 h. After the removal of free GNRs, the solution was exposed to a NIR laser (808 nm, 1 W cm^{-2}). 5 μL of the diluted (100 times) bacteria culture (before or after laser treatment) was dropped and dried on a copper grid for TEM observation.

Results and discussion

In this study, we used tri-thiomannoside as a sugar motif for bacterial protein targeting. These sugar clusters were synthesized by a thiol–ene click strategy;[36] an ethylene glycol side chain with a terminal mercapto group was introduced *via* a conventional acid–amine coupling reaction using EDC/HOBT reagents and deacetylation was finally carried out to afford Man_3-SH (Scheme S1, S6 and S7†). The structure of trimannoside cluster immobilized GNR (Man_3-GNR) used in this study is presented in Fig. 1. The introduction of a polyethylene glycol spacer is helpful for increasing water solubility because of its ability to stabilize the assembled nanostructures in aqueous media.

Synthesis and characterization of glycan-functionalized GNRs

The GNRs used in this study are Raman-encoded, Ag coated Au nanorods. The Raman dye, 4-nitrothiophenol, was added during the silver deposition process (see the Experimental section); therefore, the GNRs were rendered Raman-active after

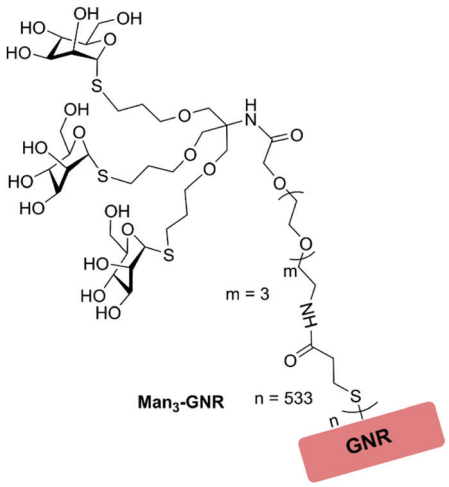

Fig. 1 Structure of tri-thiomannoside modified GNRs (Man_3-GNRs) used in this study, where n = 533 represents the number of glycoclusters covalently attached on each GNR.

Open Access Article. Published on 26 March 2018. Downloaded on 5/7/2026 1:40:22 AM.
This article is licensed under a Creative Commons Attribution-NonCommercial 3.0 Unported Licence.

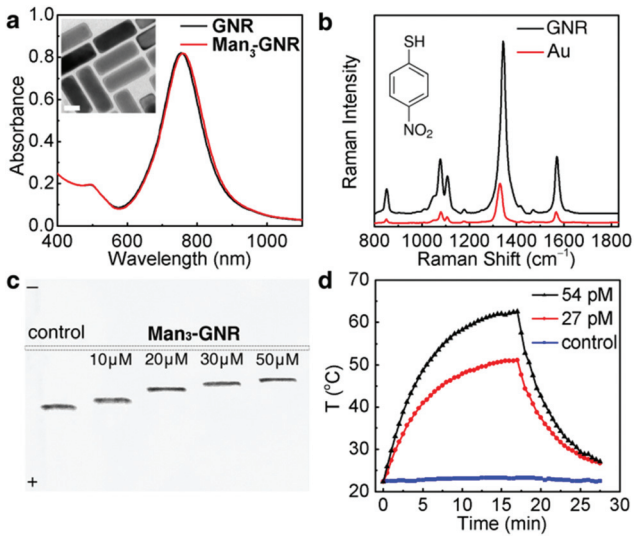

Fig. 2 (a) Absorption spectra of pristine GNR (Raman-encoded Au@Ag nanorods) and Man_3-GNR; the inset is the TEM Image of Man_3-GNR. (b) Raman scattering spectra of 4-nitrothiophenol-encoded Au nanorods and GNRs. (c) Electrophoresis results of control (pristine GNR) and Man_3-GNR at different concentrations of Man_3-SH. (d) Photothermal effect of Man_3-GNR in water upon irradiation by NIR laser light (808 nm) with different Man_3-GNR concentrations.

the synthesis. The absorption spectrum of the obtained GNRs (Fig. 2a) was characterized using a longitudinal LSPR peak at 750 nm. After being glycan-functionalized with Man_3-SH, the absorption spectrum experienced a slight red-shift to 753 nm because of the change in refractive index due to the ligands.[37] There is no peak broadening after surface-modification, indicating that the obtained nanorods (denoted by Man_3-GNR) are stable in water without aggregation. The average number of Man_3-SH on each nanorod was determined to be 533 based on Ellman's assay (Fig. S4†). Fig. 2b shows a Raman spectrum of the Man_3-GNR with characteristic Raman peaks of 4-nitrothiophenol (black line). In comparison, pure Au nanorods without silver coating show a much weaker Raman intensity, highlighting the advantage of using the core–shell GNRs.

The original SDS stabilized GNRs are negatively charged with a zeta potential of −25 mV. After surface-modification, the zeta potential dropped to −19 mV. Electrophoresis results (Fig. 2c) show decreasing electrophoresis mobility with increasing concentrations of Man_3-SH added into the GNR solution. As the introduction of Man_3-SH does not cause aggregation of the GNRs, the reduced electrophoresis mobility should result from the decrease of surface charges. Meanwhile, the electrophoresis bands are very narrow, confirming the monodispersity and excellent stability of the glycan-functionalized GNRs. The GNRs were further tested for their photothermal properties using a NIR laser (808 nm, 1 W cm^{-2}). Two concentrations of Man_3-GNR, 27 pM and 54 pM, with absorbances of 0.5 and 1 respectively at 808 nm, were tested by a heating and cooling process (Fig. 2d). The solution was irradiated to reach equilibrium temperatures of 51 °C and 65 °C respectively for absorbances of 0.5 and 1. In comparison, pure water did not show an obvious temperature increase after laser irradiation. Based on the heating–cooling curves, the photothermal efficiency of Man_3-GNR at 808 nm was estimated to be 49.3%.

Specificity and efficiency in recognition of Man_3-GNR with ConA

We first investigated the recognition between Man_3-GNR and a model mannose-recognizing lectin, *i.e.* ConA.[38] Absorption spectra of Man_3-GNR solutions were measured after mixing with different concentrations of ConA (Fig. 3a). Binding of GNRs with ConA resulted in broadening and red-shift of the LSPR peak, a result of plasmon coupling between adjacent GNRs in the aggregates formed.[39] With the increase of the ConA concentration, the nanorods experienced severer aggregation, indicated by the red-shift and broadening of the LSPR peak.[40,41] To prove that the spectral change was indeed due to recognition between ConA and mannose, galactose-cluster functionalized GNRs (Gal_3-GNR) were also synthesized as a control. Within the same ConA concentration range, there were no obvious changes in the absorption spectra after introducing ConA (Fig. 3b). Furthermore, mannose solutions with high concentrations (20 mM and 50 mM) were mixed with Man_3-GNR for competitive binding to ConA. With the increase of the mannose concentration, lesser extents of red-shifts of the LSPR peak were observed, suggesting less aggregation of the GNRs (Fig. 3c). Dynamic light scattering (DLS) measurements were also performed to determine the aggregation states of the nanorods (Fig. S9†), which agreed well with the

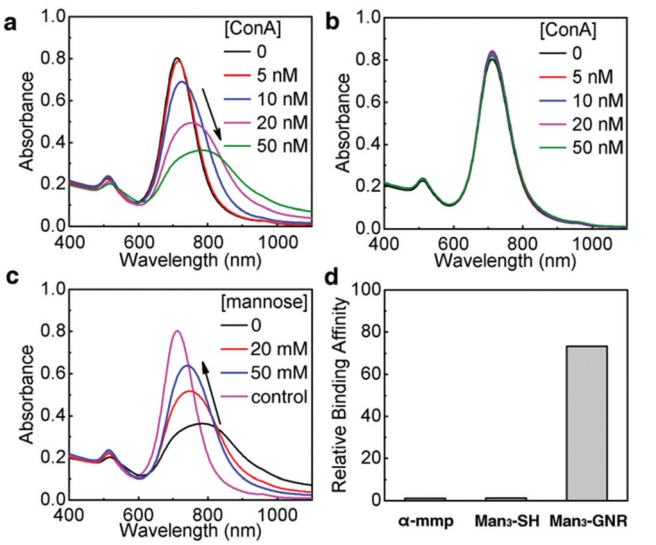

Fig. 3 (a) Absorption spectra of Man3-GNR with various concentrations of ConA. (b) Absorption spectra of Gal3-GNR with various concentrations of ConA. (c) Absorption spectra of Man3-GNR with different concentrations of mannose after the addition of ConA (50 nM). (d) Relative binding affinity to ConA determined by ITC for methyl-α-D-mannopyranoside (α-mmp), Man3-SH and Man3-GNR (mannose molar concentration bases).

This journal is © The Royal Society of Chemistry 2018

Open Access Article. Published on 26 March 2018. Downloaded on 5/7/2026 1:40:22 AM.
This article is licensed under a Creative Commons Attribution-NonCommercial 3.0 Unported Licence.

results obtained from the absorption spectra. These results substantiate the high specificity of Man_3-GNR binding to ConA.

ITC titration experiments were performed between ConA and Man_3-SH to examine the binding affinity of the trimeric mannosides with ConA using methyl α-D-mannopyranoside (α-mmp) as the control; α-mmp is well-known to bind to ConA.[42] The ITC titrations give an association constant of 8.79×10^3 M^{-1} (per mannose base) for ConA and Man_3-SH, and a K_1 of 7.50×10^3 M^{-1} with α-mmp. Notably, the addition of a low concentration of Man_3-GNR (30 nM) into α-mmp (1 : 41.6 Man_3-GNR : α-mmp based on the mannose molar concentration) with ConA led to considerably increased affinity (Fig. S7†). The obtained binding constant for the two ligand mixture gave rise to the binding constant of Man_3-GNR recognition with ConA of $K_2 = 551 \times 10^3$ M^{-1}. This experiment confirmed the excellent multivalency effect of Man_3-GNR in binding to ConA and gave the relative binding affinity of α-mmp and Man_3-GNR = 1 : 72 (Fig. 3d, mannose molar concentration bases). Furthermore, the ITC of the ligand–ligand titration between α-mmp and Man_3-GNR, and Gal_3-GNR with ConA confirms no binding.

Confirmation of FimH-specific binding of Man_3-NH-rhodamine

We next examine the selective recognition of this glycan modified GNR to bacteria (*E. coli* UTI89). Among the different species of pathogenic bacteria, *E. coli* are among the major species[43,44] that initiate the damage and pathological changes in the gastrointestinal and urinary systems.[45,46] UPEC is the most common pathogenic agent to cause urinary tract infections.[47] The FimH expression of most of the *E. coli* bacteria mediates the mannose sensitive binding to target host cells.[48] Fimbriae of *E. coli* have been shown to facilitate bacterial colonization and invasion of human bladder cells.[49] A wide range of studies have been conducted on uropathogenic strains of *E. coli* produce type 1 fimbriae. These suggest that FimH can be a potential vaccine candidate for the prevention of infections in the urinary tract.[50]

E. coli UTI89 bacteria were genetically engineered to obtain the FimH ON and FimH OFF mutants.[51] The UTI89 FimH mutants were challenged with the glycocluster. We carried out competitive binding assay experiments by quantifying the fluorescence intensities of UTI89 bacteria treated with rhodamine dye labelled tri-thiomannoside cluster Man_3-NH-rhodamine (Scheme S8†) after they were pretreated with different concentrations of α-mmp (Fig. S3†). As the mmp concentration increases, the mannose receptors would be blocked by these α-mmp molecules so that the glycocluster does not bind to the bacteria and the measured fluorescence intensities decrease as the α-mmp concentration increases. In contrast to fimbriated *E. coli* UTI89 strains, the non-fimbriated *E. coli* UTI89 upon treatment with Man_3-NH-rhodamine does not show significant fluorescence intensity changes at different α-mmp concentrations. These experiments support the specific binding of the trimeric form of the mannoside cluster with FimH receptors of UTI89 bacterial strains.

Binding of Man_3-GNR to fimbriated *E. coli* UTI89

We investigated the binding of Man_3-GNR to UTI89 bacteria using dark field microscopy. The nanorods appear as red dots because of their light scattering in the visible spectral range, and the bacteria were characterized by a white contour. As evidenced by the dark-field images shown in Fig. 4a, the FimH-ON bacteria were clearly clustered by Man_3-GNR, while no clustering was caused for the FimH OFF bacteria (Fig. 4b). Furthermore, Gal_3-GNR nanoconjugates (Schemes S9 and S10†) did not bind to the FimH-ON bacteria (Fig. S8b†), confirming the specific binding of the mannoside cluster. A competitive assay using mannose and Man_3-GNR further proves that the binding site of the mannoside-cluster is the FimH protein (Fig. S8d†).

SERS is a sensitive and high throughput method for quantification analysis.[52,53] Different concentrations of the SERS-encoded Man_3-GNR were incubated with either FimH-ON or FimH-OFF *E. coli*. Unbound nanorods were removed by centrifugation with a filter pore size of 0.45 μm. FimH-ON UTI89 showed a concentration dependent Raman signal whereas the FimH-OFF bacterial strain showed very weak Raman signals (Fig. 4c and d). The dependence of the SERS intensity at 1340 cm^{-1} on the concentration of Man_3-GNR is plotted as shown in the inset of Fig. 4c. By fitting the curve according to the Hill equation,[54] the binding affinity of Man_3-GNR with FimH-ON UTI89 bacteria was found to be 1.08×10^{10} M^{-1} based on the GNR concentration (or 6.72×10^6 M^{-1} based on the mannose concentration). It is interesting to note that this value is two orders of magnitude larger than the binding affinity of FimH with natural high-mannose *N*-glycans (estimated to be 5×10^4 M^{-1}).[55] We also incubated different concentrations of FimH-ON bacteria with 0.25 nM Man_3-GNR and measured the Raman spectra (Fig. S10†). *E. coli* at a concentration of 10^3 CFU mL^{-1} could be detected.

Selective killing of fimbriated *E. coli* UTI89

After confirming that Man_3-GNR can bind to fimbriated *E. coli* with high affinity, we tested if selective bacterial killing is possible. Both FimH-ON and FimH-OFF bacteria were incubated with Man_3-GNR for 1 h. After removing the unbound nanorods, the solution was exposed to an 808 nm laser. After irradiation for 15 min, the number of live cells was determined by plating the bacteria on LB plates, which were then incubated at 37 °C for 24 h. As shown in Fig. 4e, nearly all FimH-ON bacteria (99.98%) were dead when 0.2 nM Man_3-GNR was used. Without laser irradiation, the FimH-ON *E. coli* were also inhibited by 26%, most likely due to the intrinsic antibacterial activity of Ag in the GNRs.[56] In contrast, the viability of FimH-OFF *E. coli* was much higher after the same treatment (Fig. 4f). The difference in the killing efficiency of the two bacterial strains highlights the significance of targeted binding in specific antibacterial activity.

Live/dead analysis using SYTO 9 and propidium iodide (PI) was performed to visualize the extent of killing of bacteria with the treatment of Man_3-GNR (0.2 nM) with or without laser

Open Access Article. Published on 26 March 2018. Downloaded on 5/7/2026 1:40:22 AM.
This article is licensed under a Creative Commons Attribution-NonCommercial 3.0 Unported Licence.

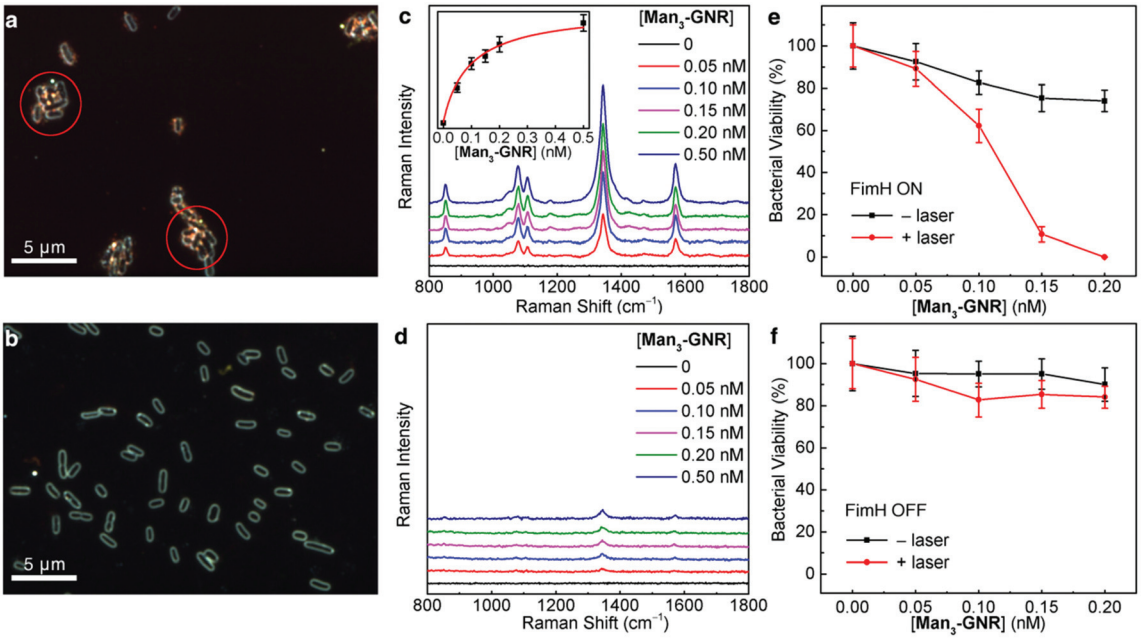

Fig. 4 Binding and killing of *E. coli* UTI89 bacteria by Man_3-GNR. (a, b) Dark field microscopy images of FimH-ON (a) and FimH-OFF (b) bacteria treated with Man_3-GNR. Red circles indicate larger bacteria clusters with Man_3-GNR due to multivalent interaction of Man_3-GNR with FimH-ON UTI89. (c, d) Raman spectra of Man_3-GNR treated FimH-ON (c) and FimH-OFF (d) bacteria. (e, f) Bacterial viability of FimH-ON (e) and FimH-OFF (f) UTI89 treated with Man_3-GNR and laser irradiation.

irradiation for both FimH-ON and FimH-OFF *E. coli* strains (Fig. 5). Dead cells and live cells show red and green fluorescence, respectively. The FimH-ON bacteria were almost completely stained red after laser irradiation for 15 min (Fig. 5b). Live bacteria along with some amount of killed bacteria were observed in non-treatment control and FimH-OFF *E. coli* strain. These results are consistent with the bacterial viability data obtained by CFU counting (Fig. 4e and f). Meanwhile, the staining assay confirms that there is membrane damage after the treatment because the cell-impermeant PI dye stained the cells.

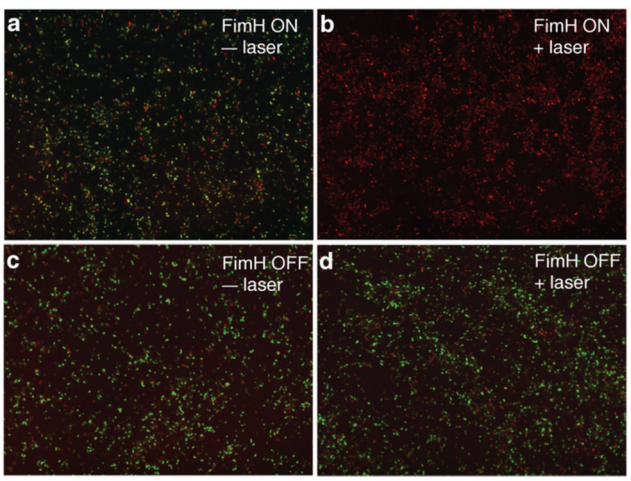

Fig. 5 Fluorescence images of UTI89 bacteria under different conditions: (a) Man_3-GNR bound FimH-ON bacteria without laser treatment, (b) FimH-ON bacteria after laser irradiation, (c) FimH-OFF bacteria without NIR treatment after removing unbound Man_3-GNR, and (d) FimH-OFF bacteria after laser irradiation.

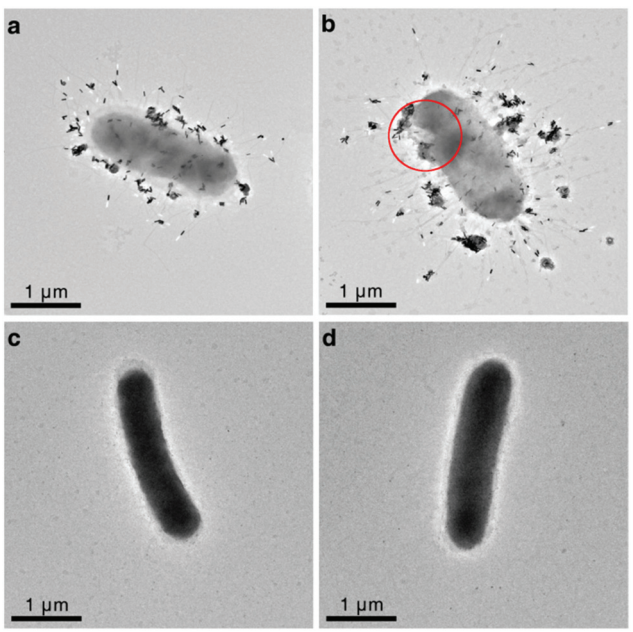

Fig. 6 Transmission electron microscopy (TEM) images of *E. coli* UTI89 bacteria treated with 0.2 nM Man_3-GNR under different conditions: (a) FimH ON, before laser irradiation; (b) FimH ON, after laser irradiation; (c) FimH OFF, before laser irradiation; and (d) FimH OFF, after laser irradiation. The red circle in (b) shows membrane damage.

This journal is © The Royal Society of Chemistry 2018

Open Access Article. Published on 26 March 2018. Downloaded on 5/7/2026 1:40:22 AM.
This article is licensed under a Creative Commons Attribution-NonCommercial 3.0 Unported Licence.

Finally, we examined the morphology changes of the UTI89 bacteria after Man_3-GNR binding and laser treatment using transmission electron microscopy (TEM). Single bacteria instead of clustered bacteria were imaged for clarity. The TEM images clearly show that the FimH-ON bacteria are fimbriated (Fig. 6a and b) while the FimH OFF bacteria are not (Fig. 6c and d), and Man_3-GNR specifically bind to fimbriated bacteria. Fig. 6a and b further confirm that the nanorods bind to the fimbriae rather than the cell walls of the bacteria. The number of nanorods per bacterium is over 100, which is expected to release intense heat locally to the bacteria when irradiated by light. It is evidenced in Fig. 6b that rupture of bacterial membrane occurs after laser treatment. No clear changes were observed for the FimH-OFF bacteria after laser irradiation, which is expected because bacteria without GNR attachment do not absorb NIR light.

Conclusions

We have demonstrated the specific multivalent binding of trithiomannoside cluster modified GNRs to fimbriated *E. coli* as a well-defined model system. The glycan-functionalized GNRs can be utilized for targeted detection and killing of *E. coli*. The glycan cluster modified GNRs showed efficient recognition with both ConA and FimH of *E. coli* UTI89. Dark-field imaging and SERS detection clearly differentiated FimH-ON and FimH-OFF bacterial strains. Furthermore, by employing the photothermal properties of the plasmonic nanoconjugates, specific killing of fimbriated *E. coli* bacteria could be achieved. Our design of multivalent glyco-nanoparticles is of potential for *in vivo* applications for UTI and recurrent UTI.

Conflicts of interest

There are no conflicts to declare.

Acknowledgements

This work was funded and supported by Ministry of Education-Singapore (MOE2013-T3-1-002 and RG49/16), and a Singapore MOH Industry Alignment Fund (NMRC/MOHIAFCAT2/003/2014). The *E. coli* strains UTI89, SLC-490, and SLC-492 were kindly provided by Lu Ting Liow and Swaine Chen.

Notes and references

1 A. Varki, *Essentials of glycobiology*, Cold Spring Harbor Laboratory Press, Cold Spring Harbor, N.Y., 2009.
2 A. K. Adak, H.-J. Lin and C.-C. Lin, *Org. Biomol. Chem.*, 2014, **12**, 5563–5573.
3 J. J. Lundquist and E. J. Toone, *Chem. Rev.*, 2002, **102**, 555–578.
4 M. Marradi, F. Chiodo, I. García and S. Penadés, *Chem. Soc. Rev.*, 2013, **42**, 4728–4745.
5 Z. Qi, P. Bharate, C. H. Lai, B. Ziem, C. Böttcher, A. Schulz, F. Beckert, B. Hatting, R. Mülhaupt, P. H. Seeverger and R. Haag, *Nano Lett.*, 2015, **15**, 6051–6057.
6 X. Li and G. Chen, *Polym. Chem.*, 2015, **6**, 1417–1430.
7 M. Gómez-García, J. M. Benito, D. Rodríguez-Lucena, J.-X. Yu, K. Chmurski, C. O. Mellet, R. G. Gallego, A. Maestre, J. Defaye and J. M. G. Fernández, *J. Am. Chem. Soc.*, 2005, **127**, 7970–7971.
8 C.-C. Lin, Y.-C. Yeh, C.-Y. Yang, C.-L. Chen, G.-F. Chen, C.-C. Chen and Y.-C. Wu, *J. Am. Chem. Soc.*, 2002, **124**, 3508–3509.
9 F. Manea, C. Bindoli, S. Fallarini, G. Lombardi, L. Polito, L. Lay, R. Bonomi, F. Mancin and P. Scrimin, *Adv. Mater.*, 2008, **20**, 4348–4352.
10 K. El-Boubbou, C. Gruden and X. Huang, *J. Am. Chem. Soc.*, 2007, **129**, 13392–13393.
11 L. Lartigue, C. Innocenti, T. Kalaivani, A. Awwad, M. Sanchez Duque, Y. Guari, J. Larionova, C. Guérin, J.-L. Georges Montero, V. Barragan-Montero, P. Arosio, A. Lascialfari, D. Gatteschi and C. Sangregorio, *J. Am. Chem. Soc.*, 2011, **133**, 10459–10472.
12 C.-H. Lai, C.-Y. Lin, H.-T. Wu, H.-S. Chan, Y.-J. Chuang, C.-T. Chen and C.-C. Lin, *Adv. Funct. Mater.*, 2010, **20**, 3948–3958.
13 A. Cambi, D. S. Lidke, D. J. Arndt-Jovin, C. G. Figdor and T. M. Jovin, *Nano Lett.*, 2007, **7**, 970–977.
14 I. García, A. Sánchez-Iglesias, M. Henriksen-Lacey, M. Grzelczak, S. Penadés and L. M. Liz-Marzán, *J. Am. Chem. Soc.*, 2015, **137**, 3686–3692.
15 M. Khanal, F. Larsonneur, V. Raks, A. Barras, J.-S. Baumann, F. A. Martin, R. Boukherroub, J.-M. Ghigo, C. O. Mellet, V. Zaitsev, J. M. G. Fernandez, C. Beloin, A. Siriwardena and S. Szunerits, *Nanoscale*, 2015, **7**, 2325–2335.
16 B. M. Illescas, J. Rojo, R. Delgado and N. Martín, *J. Am. Chem. Soc.*, 2017, **139**, 6018–6025.
17 A. Barras, F. A. Martin, O. Bande, J. S. Baumann, J.-M. Ghigo, R. Boukherroub, C. Beloin, A. Siriwardena and S. Szunerits, *Nanoscale*, 2013, **5**, 2307–2316.
18 J. Wei, L. Zheng, X. Lv, Y. Bi, W. Chen, W. Zhang, Y. Shi, L. Zhao, X. Sun, F. Wang, S. Cheng, J. Yan, W. Liu, X. Jiang, G. F. Gao and X. Li, *ACS Nano*, 2014, **8**, 4600–4607.
19 M. Reynolds, M. Marradi, A. Imberty, S. Penadés and S. Perez, *Chem. – Eur. J.*, 2012, **18**, 4264–4273.
20 X. Wang, E. Matei, A. M. Gronenborn, O. Ramström and M. Yan, *Anal. Chem.*, 2012, **84**, 4248–4252.
21 C.-C. Lin, Y.-C. Yeh, C.-Y. Yang, G.-F. Chen, Y.-C. Chen, Y.-C. Wu and C.-C. Chen, *Chem. Commun.*, 2003, 2920–2921.
22 H. Chen, L. Shao, Q. Li and J. Wang, *Chem. Soc. Rev.*, 2013, **42**, 2679–2724.
23 X. Xu, Y. Chen, H. Wei, B. Xia, F. Liu and N. Li, *Anal. Chem.*, 2012, **84**, 9721–9728.

Open Access Article. Published on 26 March 2018. Downloaded on 5/7/2026 1:40:22 AM.
This article is licensed under a Creative Commons Attribution-NonCommercial 3.0 Unported Licence.

24 L. A. Lane, X. Qian and S. Nie, *Chem. Rev.*, 2015, **115**, 10489–10529.
25 H. Zhang, X. Ma, Y. Liu, N. Duan, S. Wu, Z. Wang and B. Xu, *Biosens. Bioelectron.*, 2015, **74**, 872–877.
26 Z. Wang, S. Zong, L. Wu, D. Zhu and Y. Cui, *Chem. Rev.*, 2017, **117**, 7910–7963.
27 J. Langer, I. García and L. M. Liz-Marzán, *Faraday Discuss.*, 2017, **205**, 363–375.
28 T. Ming, H. Chen, R. Jiang, Q. Li and J. Wang, *J. Phys. Chem. Lett.*, 2012, **3**, 191–202.
29 Y. Zhu, M. Ramasamy and D. K. Yi, *ACS Appl. Mater. Interfaces*, 2014, **6**, 15078–15085.
30 J. D. Schilling, M. A. Mulvey and S. J. Hultgren, *J. Infect. Dis.*, 2001, **183**, S36–S40.
31 M. G. Blango and M. A. Mulvey, *Antimicrob. Agents Chemother.*, 2010, **54**, 1855–1863.
32 B. Foxman, *Infect. Dis. Clin. North Am.*, 2014, **28**, 1–13.
33 A. L. Flores-Mireles, J. N. Walker, M. Caparon and S. J. Hultgren, *Nat. Rev. Microbiol.*, 2015, **13**, 269–284.
34 C. N. Spaulding, R. D. Klein, S. Ruer, A. L. Kau, H. L. Schreiber, Z. T. Cusumano, K. W. Dodson, J. S. Pinkner, D. H. Fremont, J. W. Janetka, H. Remaut, J. I. Gordon and S. J. Hultgren, *Nature*, 2017, **546**, 528–532.
35 H. Chen, L. Shao, T. Ming, Z. Sun, C. Zhao, B. Yang and J. Wang, *Small*, 2010, **6**, 2272–2280.
36 A. B. Lowe, *Polym. Chem.*, 2014, **5**, 4820–4870.
37 K. M. Mayer and J. H. Hafner, *Chem. Rev.*, 2011, **111**, 3828–3857.
38 J. H. Naismith and R. A. Field, *J. Biol. Chem.*, 1996, **271**, 972–976.
39 P. K. Jain, S. Eustis and M. A. El-Sayed, *J. Phys. Chem. B*, 2006, **110**, 18243–18253.
40 S.-J. Richards, L. Otten and M. I. Gibson, *J. Mater. Chem. B*, 2016, **4**, 3046–3053.
41 X.-L. Hu, H.-Y. Jin, X.-P. He, T. D. James, G.-R. Chen and Y.-T. Long, *ACS Appl. Mater. Interfaces*, 2015, **7**, 1874–1878.
42 S. L. Mangold and M. J. Cloninger, *Org. Biomol. Chem.*, 2006, **4**, 2458–2465.
43 A. Ronald, *Dis.-Mon.*, 2003, **49**(2), 71–82.
44 J. B. Kaper, J. P. Nataro and H. L. T. Mobley, *Nat. Rev. Microbiol.*, 2004, **2**, 123–140.
45 H. M. Zowawi, P. N. A. Harris, M. J. Roberts, P. A. Tambyah, M. A. Schembri, M. D. Pezzani, D. A. Williamson and D. L. Paterson, *Nat. Rev. Urol.*, 2015, **12**, 570–584.
46 L. J. Grauke, I. T. Kudva, J. W. Yoon, C. W. Hunt, C. J. Williams and C. J. Hovde, *Appl. Environ. Microbiol.*, 2002, **68**, 2269–2277.
47 K. J. Wright, P. C. Seed and S. J. Hultgren, *Cell. Microbiol.*, 2007, **9**, 2230–2241.
48 S. G. Stahlhut, V. Tchesnokova, C. Struve, S. J. Weissman, S. Chattopadhyay, O. Yakovenko, P. Aprikian, E. V. Sokurenko and K. A. Krogfelt, *J. Bacteriol.*, 2009, **191**, 6592–6601.
49 A. L. Flores-Mireles, J. N. Walker, M. Caparon and S. J. Hultgren, *Nat. Rev. Microbiol.*, 2015, **13**, 269–284.
50 M. A. Schembri, H. Hasman and P. Klemm, *FEMS Microbiol. Lett.*, 2000, **188**, 147–151.
51 S. L. Chen, C. S. Hung, J. S. Pinkner, J. N. Walker, C. K. Cusumano, Z. Li, J. Bouckaert, J. I. Gordon and S. J. Hultgren, *Proc. Natl. Acad. Sci. U. S. A.*, 2009, **106**, 22439–22444.
52 H.-Y. Lin, C.-H. Huang, W.-H. Hsieh, L.-H. Liu, Y.-C. Lin, C.-C. Chu, S.-T. Wang, I.-T. Kuo, L.-K. Chau and C.-Y. Yang, *Small*, 2014, **10**, 4700–4710.
53 D. Craig, S. McAughtrie, J. Simpson, C. McCraw, K. Faulds and D. Graham, *Anal. Chem.*, 2014, **86**, 4775–4782.
54 C. Röcker, M. Pötzl, F. Zhang, W. J. Parak and G. U. Nienhaus, *Nat. Nanotechnol.*, 2009, **4**, 577–580.
55 D. Kisiela, A. Laskowska, A. Sapeta, M. Kuczkowski, A. Wieliczko and M. Ugorski, *Microbiology*, 2006, **152**, 1337–1346.
56 X. Ding, P. Yuan, N. Gao, H. Zhu, Y. Y. Yang and Q.-H. Xu, *Nanomedicine*, 2017, **13**, 297–305.

This journal is © The Royal Society of Chemistry 2018